

Coupled Aggregation and Sedimentation Processes: Three Dimensional Off-Lattice Simulations

R. Leone¹, G. Odriozola¹, L. Mussio¹, A. Schmitt², and R. Hidalgo-Álvarez²^a

¹ Departamento de Química Física y Matemática, Facultad de Química
Universidad de la República, 11800 Montevideo, Uruguay

² Departamento de Física Aplicada; Universidad de Granada;
Campus de Fuentenueva; E-18071 Granada; Spain

Received: date / Revised version: date

Abstract. The coupled aggregation and sedimentation process were studied by means of three dimension computer simulations. For this purpose, a large prism with no periodic boundary conditions for the sedimentation direction was considered. Furthermore, three equally sized and mutually excluded regions were defined inside the prism, a top, a middle and a bottom region. This allows to study the time evolution of the cluster size distribution and the cluster structure for each region. The mass distribution profile and the center of mass position were also accessed as a function of time. For the bottom region, the effects of the sediment formation on the kinetics of growth and on the cluster structure were clearly observed. The obtained results not only agree with the experimental data obtained by Allain et. al. [1] and with the simulations made by Gonzalez [2] but also allow to gain further in the details.

PACS. 82.70.Dd Colloids – 82.20.Mj Nonequilibrium kinetics – 02.50.-r Probability theory, stochastic processes and statistics

1 Introduction

In a larger or smaller extent, all real aggregation processes are influenced by the presence of an external gravitational field. Hence, the aggregation phenomena are usually followed by sedimentation or, in many cases, both are present simultaneously. Some natural examples are the delta formation at a river discharge into the ocean and the settling of bacteria clusters in quiet water [3]. As technological examples one may cite the water treatment for human consumption (clarifying), effluents treatment, and a large number of precipitation techniques employed by the chemical industry [4].

Pure irreversible aggregation processes have been well studied and are described in the literature. The first equation for describing the aggregation kinetics of diluted systems was written by Smoluchowski in the early 1900s [5, 6]. This equation defines an infinite two-dimensional matrix of kinetic rate constants, known as kernel, which accounts for the physical characteristics of the system. The time evolution of the cluster size distribution is obtained by solving the Smoluchowski's rate equation for a given kernel. On the other hand, much information about the aggregation processes is also contained in the clusters structure. Here, Smoluchowski's rate equation does not provide useful information and hence, other techniques

such as light scattering experiments and simulations are required for its study. Significant contributions in these fields are provided by Lin, Weitz and coworkers (light scattering experiments)[7,8,9] and Meakin, Family and Gonzalez (simulations)[10,11,12,13,14].

Pure sedimentation phenomena have also been well studied [15]. Here, an important issue is the variation of the settling velocity with the volume fraction [16,17]. When the concentrations become large enough, the reverse flow of fluid necessary to compensate the volumetric flow of particles plus the associated fluid contribute to decrease the Stokes velocity (this is known as backflow effect). Furthermore, since the volume fraction becomes larger when moving to the flask bottom, an osmotic pressure appears opposed to the gravitational field. Finally, for larger volume fractions the inter-particle distances shorten and consequently, the role of hydrodynamic forces and inter-particle interactions become important.

Although aggregation and sedimentation phenomena are closely connected, there is not an extended literature dealing with them simultaneously. This is, at least partially, due to the mathematical difficulties, which appear when following a formal analytical treatment [18]. Consequently, computer simulations become a useful alternative tool for studying and predicting the behavior of real aggregation-sedimentation systems. Recently, Gonzalez and Leyvraz worked on computer simulations for elucidating the experimental results found by Allain et. al. [1,

^a e-mail: rhidalgo@ugr.es

19]. They found that increasing the effect of the external field leads to an increase in the cluster fractal dimension. Their model, however, did not consider cluster deposition (only a sedimentation velocity was added to the Brownian motion) [20]. Later, the simulations were improved by considering a cubic lattice of size L , with periodic boundary conditions in the three spatial directions (as in the previous model), but now taking the clusters out of the cubic box with a probability related to the total distance that they had moved downwards (see ref. [2] for details). Although this model does not consider the mass distribution dependence on height, it was useful for explaining an increase of the initial particle concentration required to have gelation when sedimentation is present.

In this paper, we further study the coupled aggregation and sedimentation phenomena by simulations, but now considering a large prism with no periodical boundary conditions for the sedimentation direction (this requires a macroscopic prism height). For the other two horizontal directions, we still impose periodical boundary conditions in order to represent, in an average way, a portion of the whole system. This allows us to study not only average quantities but also their change as a function of height. Furthermore, it was possible to observe and study the sediment formation.

2 Simulation method

The simulation processes were carried out off lattice on a square section prism of side L and height H . Inside, N_0 identical hard spheres of radius a were randomly placed avoiding the overlapping among them. Since we are simulating aggregation and sedimentation processes, there are two contributions to the movement. One corresponds to the Brownian motion and the other to the Stokes sedimentation velocity. As the simulations are done for very dilute systems, the backflow and the hydrodynamic forces are not taken into account. This assumption has to be checked since local high concentrations may appear somewhere in the prism. The time step was fixed by the relationship

$$t_0 = l_B^2 / (6D_1) \quad (1)$$

where $D_1 = k_B T / (6\pi\eta a)$ is the monomer diffusion coefficient, $k_B T$ is the thermal energy, η is the solvent viscosity and l_B is the Brownian length step. Hence, monomers are always moved l_B in a random direction plus the Stokes contribution

$$l_S = v_S t_0 = l_B^2 Pe / 6a \quad (2)$$

where $v_S = 2(\rho - \rho_0)ga^2 / (9\eta)$ is the monomeric Stokes velocity, ρ is the particle density, ρ_0 is the fluid density, g is the earth gravitational constant and $Pe = 4\pi a^4 (\rho - \rho_0)g / k_B T$ is the Peclet number. For aggregates, we assume the relationship $r_g = ai^{1/d_f}$ for the radius of gyration and therefore the diffusion coefficient $D_i = k_B T i^{-1/d_f} / (6\pi\eta a)$ and the Stokes velocity $v_S = 2(\rho - \rho_0)ga^2 i^{1-1/d_f} / 9\eta$. Here, it was implicitly assumed that the hydrodynamic fractal dimension and the cluster fractal dimension are equal.

Now, in order to account for the Brownian motion, we move the aggregates l_B in a random direction only when a random number uniformly distributed in $[0,1]$, ξ , is less than the ratio between the aggregate diffusion coefficient and the monomer diffusion coefficient, i. e. when $\xi < i^{-1/d_f}$. In case that the Brownian movement is refused, the corresponding Stokes contribution

$$l_S = v_S t_0 = l_B^2 Pe i^{1-1/d_f} / 6a \quad (3)$$

is accumulated in a memory place, associated with the particular cluster, for being considered in the following time intervals. Once a Brownian contribution is accepted, the accumulated Stokes contribution is added to the cluster motion and the corresponding accumulated memory is reset to zero. Furthermore, if a given accumulated Stokes contribution exceeds a Brownian step, l_B , then the aggregate is moved downwards and the accumulated memory is also reset to zero, thus avoiding a large total step length. The algorithm minimizes the times that clusters are moved, which is the most time consuming contribution to the execution time. After any movement, the regional configuration is checked for overlaps. In case that any overlap is found, it is corrected by placing the recently moved cluster in touch with the other to form a new aggregate, i. e. diffusion limited cluster aggregation (DLCA) conditions are imposed.

Periodic boundary conditions were established for the two non sedimentation directions, x and y . Hence, the system may be understood as a small portion of a macroscopic one. However, for the sedimentation direction, z (we define the prism bottom as $z = 0$ and the prism top as $z = 1$), no periodic boundary condition was imposed in order to naturally obtain a change in properties with the prism height and a cluster deposit at the prism bottom. This forces to use of a high prism since the height of the macroscopic system coincides with its vertical length. This could be done while keeping a reasonable total number of particles, i. e. working with diluted systems. As the system symmetry was broken for the z direction, we look for this effect on the cluster populations and on the cluster structures.

For this purpose, three equally sized and mutually excluded regions were defined inside the system: a top, a middle and a bottom region. Hence, we may define a weight average cluster size for each region as

$$n_w|_h = \frac{\sum_i i^2 n_i|_h}{\sum_i i n_i|_h} \quad (4)$$

where the symbol $|_h = \text{top, middle or bottom}$ refers to the corresponding region and n_i is the number of i -sized clusters. Furthermore, the vertical position of the system center of mass is also defined as

$$z_{cm} = \frac{\sum_l i_l z_l^{cm}}{\sum_l i_l} \quad (5)$$

where i_l is the size of cluster l and z_l^{cm} is the vertical position of the center of mass of cluster l .

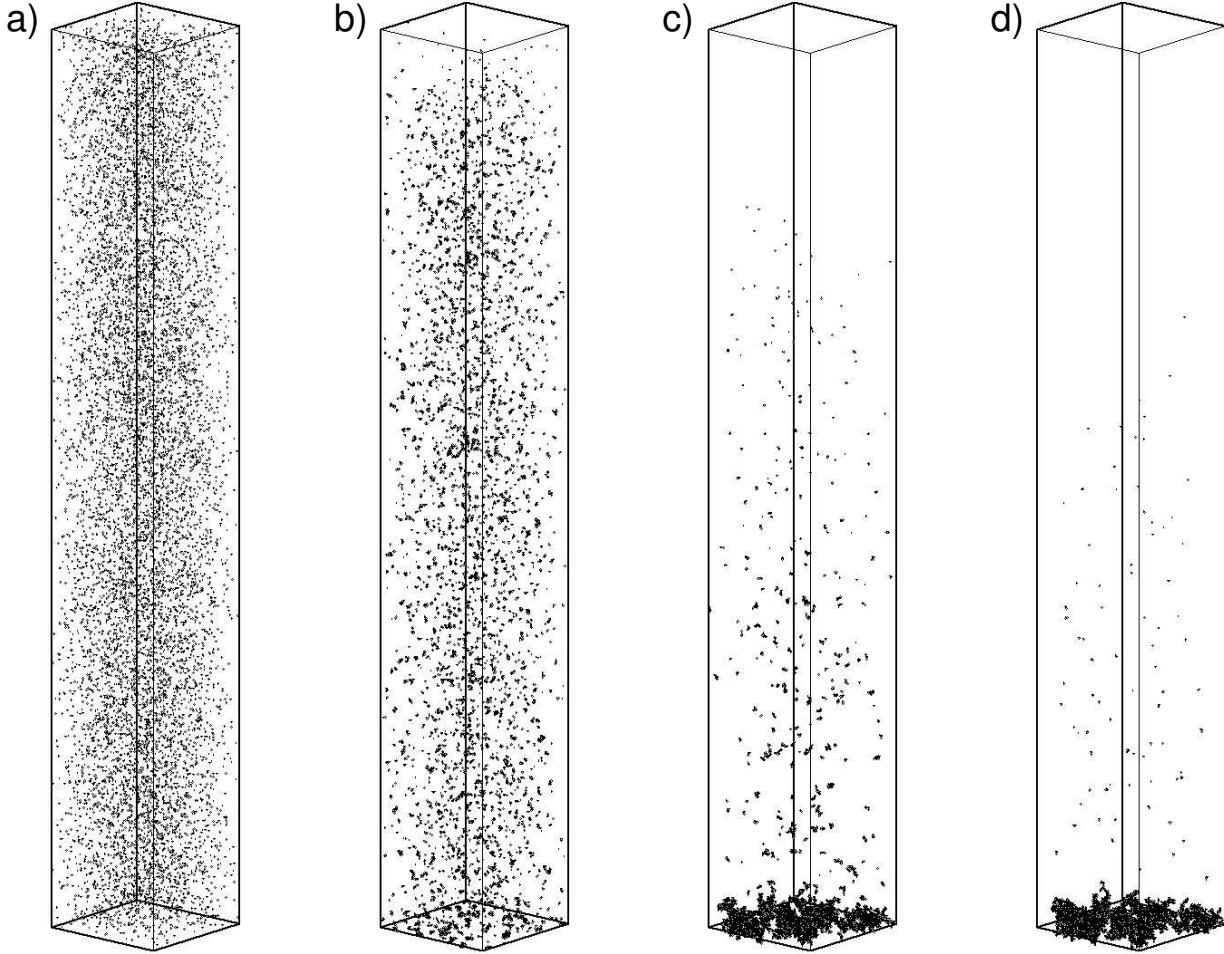


Fig. 1. Three dimensional representation of a simulated system settling under $Pe = 0.1$. The prism dimensions are $H = 1500a$ and $L = 250a$ ($H = 1500a$ was established instead of $H = 10000a$ for an easier representation). The images were captured at times 0.1 s a), 112 s b), 630 s c) and 1120 s d).

The cluster structure is studied by calculating the following radii of gyration every time a new cluster is formed

$$\begin{aligned}
 r_{gx} &= \sqrt{\frac{1}{n} \sum_i (\mathbf{r}_i \cdot \mathbf{r}_i - x_i^2)} \\
 r_{gy} &= \sqrt{\frac{1}{n} \sum_i (\mathbf{r}_i \cdot \mathbf{r}_i - y_i^2)} \\
 r_{gz} &= \sqrt{\frac{1}{n} \sum_i (\mathbf{r}_i \cdot \mathbf{r}_i - z_i^2)} \\
 r_g &= \sqrt{\frac{1}{n} \sum_i (\mathbf{r}_i \cdot \mathbf{r}_i)}
 \end{aligned} \tag{6}$$

where \mathbf{r}_i is the distance between the particle i and the cluster center of mass and x_i , y_i and z_i are its components. Those radii of gyration allow us to evaluate the average ratios $\langle r_{gx} \rangle / \langle r_{gz} \rangle |_h$ and $\langle r_{gy} \rangle / \langle r_{gz} \rangle |_h$ and to obtain three cluster fractal dimensions from $r_g |_h = a^{1/d_f |_h}$ (considering only those clusters containing more than 15 particles). The former quantities accounts for the average shape of the clusters, i. e. $\langle r_{gx} \rangle / \langle r_{gz} \rangle > 1$ indicates that the clusters tend to be elongated in the z direction and, on the contrary, $\langle r_{gx} \rangle / \langle r_{gz} \rangle < 1$ points to wider structures.

$\langle r_{gx} \rangle / \langle r_{gz} \rangle$ and $\langle r_{gy} \rangle / \langle r_{gz} \rangle$ should be similar but not equal due to statistical fluctuations and so, their difference represents an estimation of their uncertainty.

The parameters employed for the simulations are the following: a monomer radius $a = 315\text{nm}$, a Brownian step length $l_B = a/2$, a prism height $H = 10000a$, a section side $L = 250a$ and a particle volume fraction of $\phi = 6.7 \times 10^{-5}$ ($N_0 = 10000$). The particles were considered to be dispersed in water at 20^0C .

3 Results

3.1 Overview

Figure 1 was constructed to give an overview of the coupled aggregation and sedimentation processes. It shows a three dimensional representation of a system settling under $Pe = 0.1$. The images were captured from simulations at times 0.1 s a), 112 s b), 630 s c) and 1120 s d). In order to

easily represent the images, here we set $H = 1500a$ instead of $H = 10000a$, which is the value employed for the study. As can be seen for in the beginning of the process, figure 1 a) shows a uniformly distributed and monodisperse system. After a few seconds, figure 1 b), the system aggregates forming a wide cluster size distribution. As imposed, the larger clusters move faster downwards and hence, they are mostly seen close to the prism bottom. As the times goes on, those clusters start forming the sediment while the dispersion clarifies by loosing mass. The first settling aggregates that arrive to the prism bottom continue their Brownian motion although they are not allowed to move further downwards. Hence, their movement is almost restricted to two dimensions, since their weight makes difficult their upward motion. Consequently, they collide to one another forming the sediment. In the following time intervals, the system looks like the one shown in figure 1 c). Here, it is observed that the mass concentration depends on the distance from the bottom of the prism. At the top, the system is almost clear while the dispersion looks more concentrated at the bottom. Furthermore, it is also observed a large sediment that gains mass from every closed enough settling cluster. On the other hand, the number of clusters remaining in the dispersion strongly decreases and the aggregation rate of the dispersion slows down. Consequently, aggregation becomes highly improbable for those small remaining clusters and a long time is needed for their deposition. This situation is clearly seen in figure 1 d).

It should be pointed out that this first overview is in good agreement with the experimental observations made by Allain et. al. for calcium carbonate colloidal suspensions [1]. Their observations were performed experimentally in a 800 mm high cell. Furthermore, they emphasize that the different phases of settling cannot be identified separately for smaller cells. This is not surprising since their experiments were characterized by a Peclet number close to 10^{-5} .

3.2 Further inside in the details

Figure 2 a) shows the time evolution of the cluster-size distribution for the upper portion of the system, $h = \text{top}$, aggregating under $Pe = 0.1$. As expected, the first stage of the aggregation process evolves in time similarly to the DLCA regime, i. e. the sedimentation effects are not yet important. Once oligomer concentration becomes higher, the subsystem starts loosing mass due to their sedimentation making impossible the formation of larger clusters. Furthermore, the characteristic bell shape evolutions of oligomers narrow since they disappear not only by reaction but also by leaving the subsystem. When comparing the obtained time evolution of the monomer concentration with the corresponding to the DLCA regime, differences are also observed for the last stages. For pure DLCA regime, the monomeric concentration decays faster than in the case where sedimentation effects are considered due to the presence of a higher aggregation rate, which is achieved since a larger cluster concentration remains

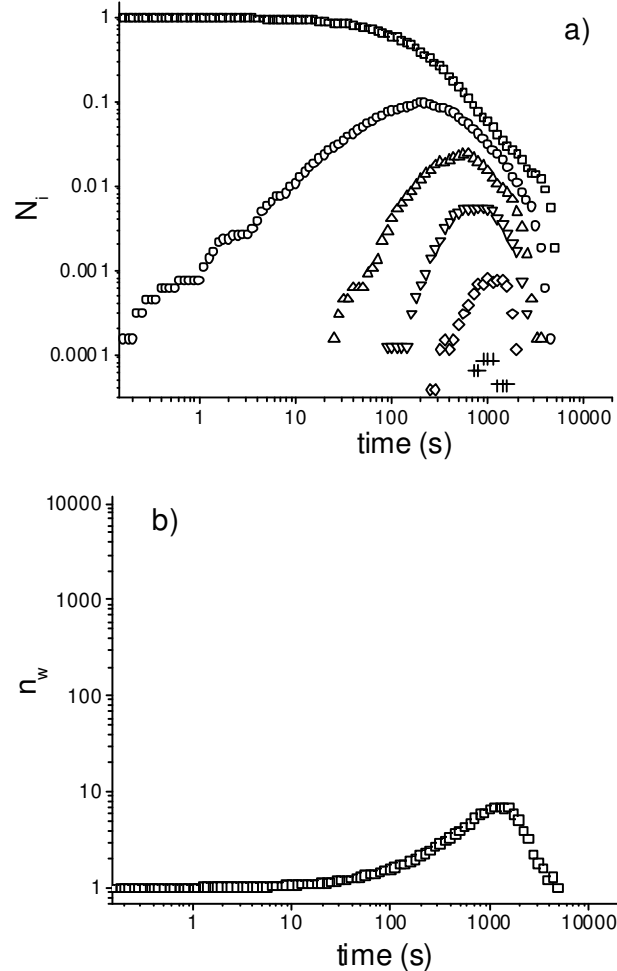


Fig. 2. a) Time evolution of the normalized cluster-size distribution for the upper portion of the system, $h = \text{top}$, and $Pe = 0.1$. The points are grouped in logarithmically spaced intervals ((\square) monomers, (\circ) 2 and 3-mers, (\triangle) 4 to 8-mers, (∇) 9 to 18-mers, (\diamond) 19 to 38-mers and (+) 39 to 88-mers. b) The corresponding weight average cluster size, n_w .

in the subsystem. Moreover, since for DLCA processes the monomeric aggregation rate constants are the largest, their curve cross the curves for the larger clusters leading to smaller monomeric concentrations [25]. This is not observed when sedimentation is present.

The corresponding weight average cluster size, n_w , for $h = \text{top}$ and $Pe = 0.1$ is shown in figure 2 b). Again, in the beginning of the processes n_w evolves in time similarly to the DLCA regime. As time goes on, two effects tends to change its evolution. On the one hand, the different sedimentation velocities of clusters make them increase their collision frequency and consequently, the average n_w tends to increase its rate of change. On the other hand, the larger aggregates exit more frequently the subsystem than the smaller ones tending to decrease the average n_w . For a given time, the second effect prevails over the former and so, the average cluster size peaks. For larger times, this

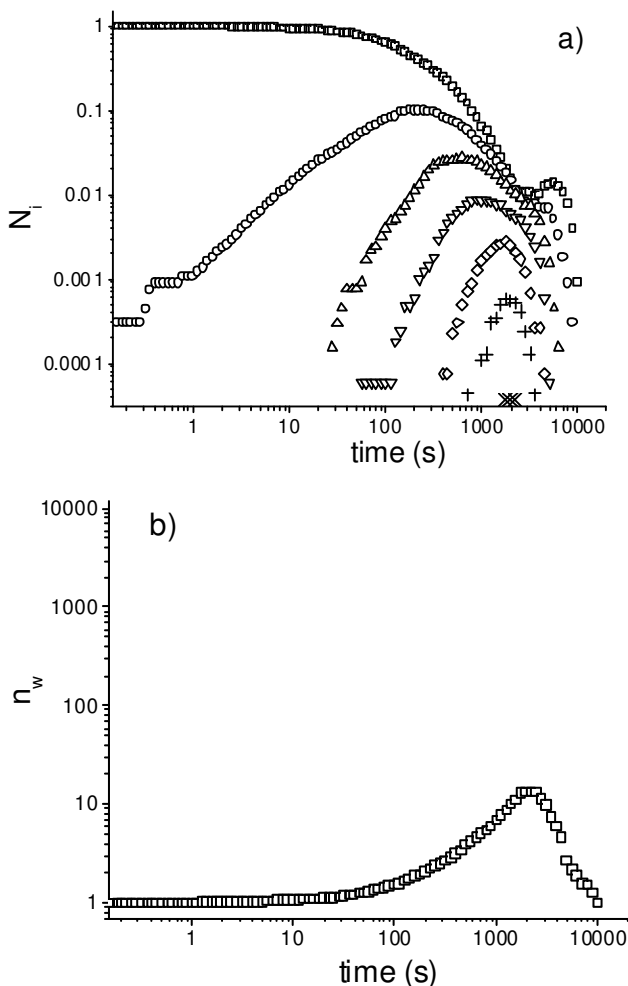


Fig. 3. a) Time evolution of the normalized cluster-size distribution for the middle portion of the system, $h = \text{middle}$ and $Pe = 0.1$. The points are grouped in logarithmically spaced intervals ((\square) monomers, (\circ) 2 and 3-mers, (\triangle) 4 to 8-mers, (∇) 9 to 18-mers, (\diamond) 19 to 38-mers, (+) 39 to 88-mers and (\times) 89 to 200-mers). b) The corresponding weight average cluster size, n_w .

situation makes the average n_w to monotonically decrease until monomers are the only species in the subsystem.

The time evolution of the cluster size distribution and the corresponding average, n_w , for the second region, $h = \text{middle}$, are shown in figure 3. Although the evolutions are similar than those shown for the upper region of the prism, some differences are found. Since this subsystem also gain mass from the upper region while loosing it towards the bottom, it is capable to develop larger structures and to hold a large number of clusters. This is clearly seen in figure 3 a) where a large number of 39 to 88-mers are shown and even a few 88 to 200-mers appears. Furthermore, the weight average cluster size peaks for larger times and reach a higher value (compare figure 3 b) with 2 b)). Finally, it is observed that monomer population becomes almost constant at approximately $t = 4000$, which is the

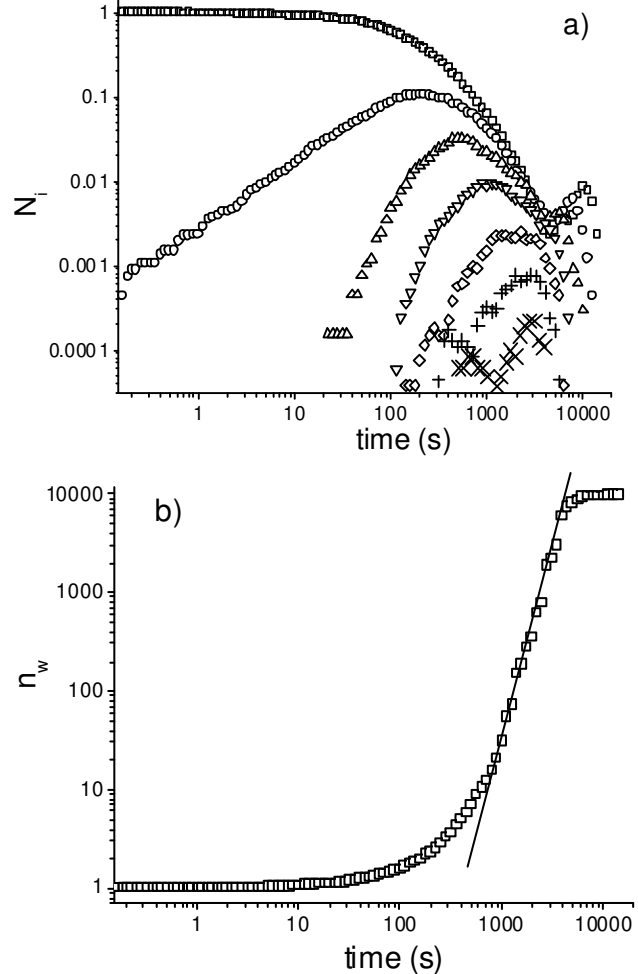


Fig. 4. a) Time evolution of the normalized cluster-size distribution for the bottom portion of the system, $h = \text{bottom}$ and $Pe = 0.1$. The points are grouped in logarithmically spaced intervals ((\square) monomers, (\circ) 2 and 3-mers, (\triangle) 4 to 8-mers, (∇) 9 to 18-mers, (\diamond) 19 to 38-mers, (+) 39 to 88-mers and (\times) 89 to 200-mers). b) The corresponding weight average cluster size, n_w .

same time at which the upper subsystem has almost lost the remaining monomers. This fact is explained by means of the monomeric transfer from the upper region towards the middle subsystem.

Figure 4 shows the time evolution of the cluster size distribution and weight average cluster size for the bottom region of the prism. Since this subsystem gains mass from the upper regions, its particle concentration continuously increases and hence, some remarkable differences appear. The most important is that the average n_w becomes a monotonously increasing function of time. Moreover, n_w seems to follow an asymptotical power behavior, $n_w \sim t^k$, where $k \simeq 4$. Due to the finite extension of the studied system, the asymptotical behavior cannot be prolonged in time and hence, n_w diminishes its rate of change until the remaining clusters settle and become part of the sediment. Another difference is that larger clusters are formed at the

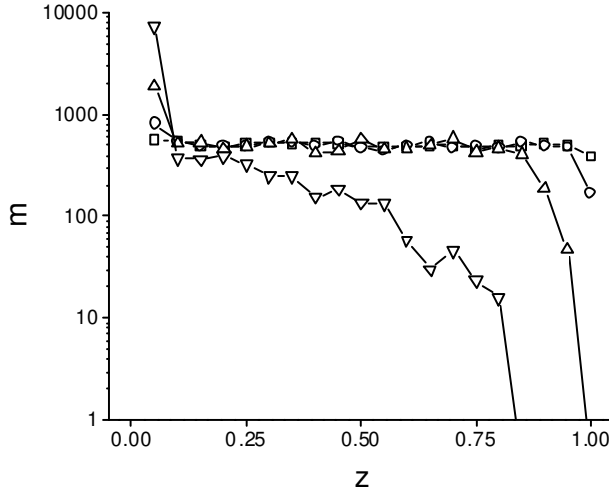


Fig. 5. Mass distribution profile, $m(z)$, along the sedimentation direction, z , represented in log-normal axes for different times. The data were obtained for $Pe = 0.1$. The symbols \square , \circ , \triangle and ∇ represent the mass distribution for $t = 112$ s, 355 s, 1122 s and 3550 s, respectively. $z = 0$ corresponds to the prism bottom and $z = 1$ to the top.

bottom faster than in the bulk. Furthermore, they also react faster to form the sediment and so, their time evolution shows a double peak. The former peak (the smallest) corresponds to those clusters aggregating at the bottom to form the sediment and the second to the bulk clusters. Monomers also behave differently. During the final stages their concentration abruptly change from diminishing to increasing. This is a consequence of the monomeric flow coming from the middle region that prevails over the small remaining aggregation rate. For even longer times, monomers eventually collide with the sediment and hence, they finally disappear.

In order to study the mass distribution profile along the sedimentation direction, z , the system was subdivided in 20 slices. For each one and for a given time, its total mass was calculated by $m(z) = \sum_i in|_z$ and represented as a point in figure 5. This figure was constructed for $Pe = 0.1$, i. e. corresponds to the data shown by figures 2, 3 and 4. It is observed for time 112 s that the mass distribution is practically uniform. Only for the upper and bottom slices, slight deviations from the mean value are observed. While the system evolves in time, those deviations becomes larger due to the settling process. At 355 s, the mass concentration of the upper slice is about one half of the initial value and the mass concentration of the bottom slice is approx. the double. The other slices, however, keep their initial mass concentration. After a sufficiently long time (see 1122 s), no remaining particles are observed in the upper slice and the mass concentration diminishes strongly in the two contiguous slices. Nevertheless, the other slices do not change their mass concentration except for the bottom one, which contains the sediment. This situation changes for very long times, where the initial mass concentration is not maintained any more in any

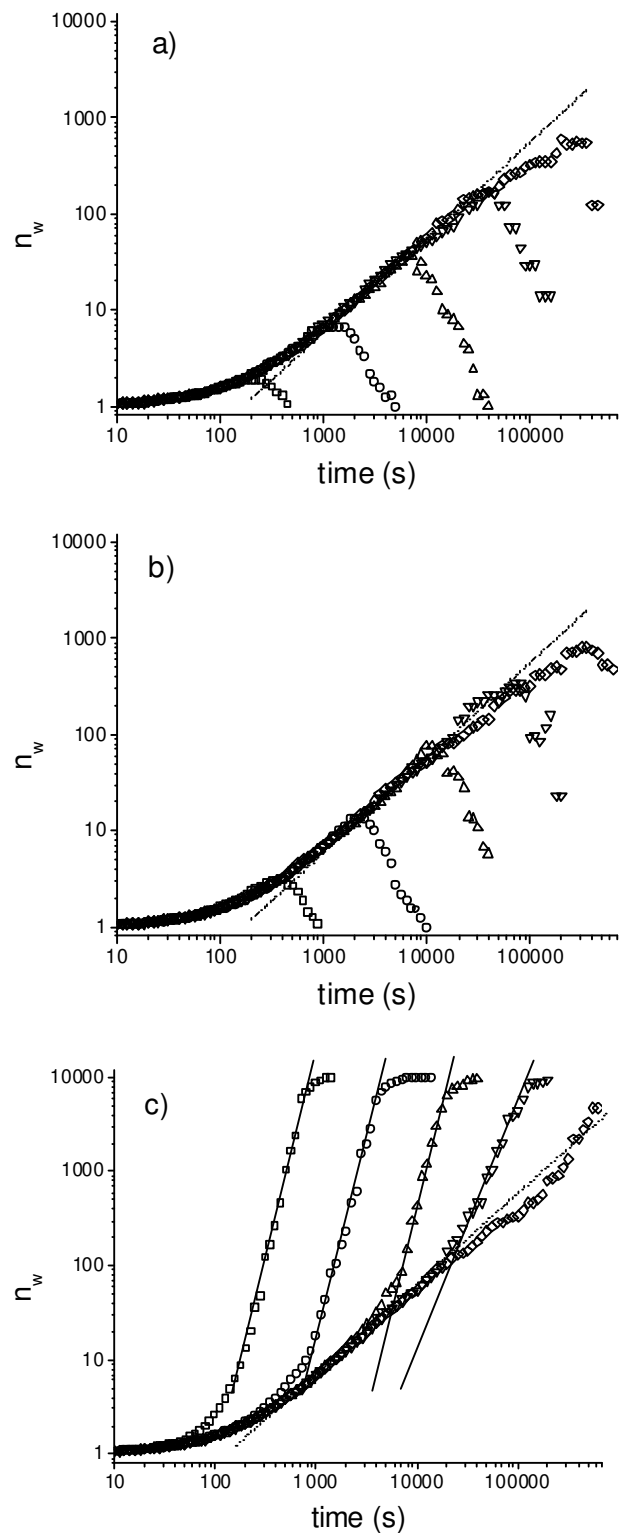


Fig. 6. Time evolutions of the weight average cluster size, n_w , for different Peclet numbers, Pe , and for the upper a), middle b), and bottom c), portions of the system. The symbols \square , \circ , \triangle , ∇ and \diamond correspond to the evolutions obtained under $Pe = 1, 0.1, 0.01, 0.001$ and 0.0001 , respectively. The dashed lines represent the asymptotical DLCA behavior. In figure c), the continuous lines are drawn as a guide to the eye.

slice of the system. This can be seen for time 3550 s. Here, the sediment contains more than half of the total mass. It should be noted that the mass concentration is not larger than the initial concentration except for the bottom slice. This means that the assumption made in section 2 of neglecting the backflow effect and the hydrodynamic forces due to the low concentration is valid for almost the whole system.

The time evolutions of the weight average cluster size, n_w , for the Peclet numbers $Pe = 1, 0.1, 0.01, 0.001$ and 0.0001 are shown in figure 6. Again, three different plots are employed for representing the evolution of each region. In addition, all figures include a unity sloped straight line, which represents the asymptotic evolution of n_w for DLCA. As expected, the sedimentation effects appears for shorter times as far the Peclet number is increased. This is clearly seen for the three prism regions. On the other hand, for the beginning of the coupled aggregation and sedimentation process and for all the studied Peclet numbers the system evolves similarly to one following a pure DLCA regime. This indicates that a very large Pe is needed for appreciating the sedimentation effects in the beginning of the processes. Figures 6 a) and b) show that the DLCA asymptotic evolution is, generally, not surpassed by the curves that consider sedimentation. In fact, when settling effects appear the weight average cluster size starts diminishing. Furthermore, it is observed for all Peclet numbers that the n_w curves peak earlier and reaching lower values for the upper region. On the contrary, in figure 6 c) it is observed that the curves behaves completely different. Here, the sedimentation effects also change the n_w evolution but strongly increasing its slope. We found for $Pe = 1, 0.1$ and 0.01 a practically constant slope of approximately 4, which is, by far, larger than the DLCA asymptotic slope. The continuous lines shown in figure 6 c) for this Peclet numbers were drawn by considering this slope. For $Pe = 0.001$ a slope of approx. 2.5 was obtained and for $Pe = 0.0001$ no significant deviation from the pure DLCA slope was observed. It is likely that, at least for our simulation conditions, the limit value of 4 is achieved for the n_w asymptotic slope.

The vertical position of the system center of mass, z_{cm} , is plotted against time in figure 7 for the set of Peclet numbers. Since the mass is randomly scattered at time zero for each system, z_{cm} takes a value closed to 0.5 at the beginning of the processes. At first stages and for all Pe , z_{cm} does not practically evolve in time. Once the aggregation process leads to large enough clusters the settling process start taking place. This starting point strongly depends on the Peclet number. The larger the Peclet number is the sooner the settling process appears since a smaller cluster size is needed for obtaining an appreciably sedimentation velocity. Once the settling effects appear, the system center of mass moves quickly towards the prism base until the mass transference from dispersion to sediment is finished.

As explained in section 2, the cluster fractal dimension was acceded by means of the radii of gyration and calculated for each defined region. For $Pe = 1$ and for the upper regions, it was not possible to obtain a reli-

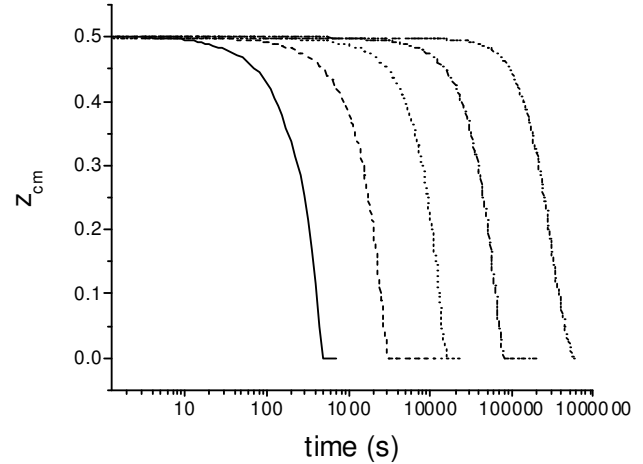


Fig. 7. a) z_{cm} as a function of time for $Pe = 1$ (solid line), 0.1 (dash line), 0.01 (dot line), 0.001 (dash-dot line) and 0.0001 (dash-dot-dot line), represented in normal-log axes.

able fractal dimension value since not enough large clusters are formed in these regions. For obtaining a reliable statistic, three simulation runs were performed for each Peclet number. Pure DLCA simulations were also carried out as a reference. The results are shown in table 1. For $Pe = 0$, i. e. pure DLCA, the values are consistent with the ones reported in the literature [21, 22]. Furthermore, no significant difference appears among the regions, as expected for a regime where no sedimentation velocity was imposed. For larger values of the Peclet number it is observed that the cluster fractal dimension increase for the top and middle regions. This is in agreement with the simulations results obtained by Gonzalez, in which no extra effects are needed, such us cluster restructuring, in order to found an increase of the fractal dimension [2]. Nevertheless, Gonzalez obtained $d_f = 2.27$ for the larger structures and for $Pe = 0.01$, which is larger than our results. This may be a consequence of the higher concentrations employed in his simulations as discussed further in the text. In addition, the $d_f|_{middle}$ values seems to be slightly larger than the $d_f|_{top}$ values. This may be due to the average downward distance that the corresponding clusters moved. Since this distance is longer for the clusters inside the middle region, the effect of increasing the fractal dimension due to the Stokes velocity becomes more evident.

The fractal dimensions obtained for the bottom region varies in a quite different way with the Peclet number than for the upper regions. Here, it is observed that d_f strongly decreases as the Peclet number increases. It was expected, however, to obtain even larger fractal dimensions than the ones obtained for the upper regions. The fact of obtaining a fractal dimension as low as $d_f = 1.68 \pm 0.05$ for $Pe = 1$ clearly indicates that the sediment formation is changing in some way the growth process. Since the cluster movement is restricted almost to two dimensions at the prism base and since the fractal dimension yield for DLCA processes at two dimensions is $d_f = 1.45 \pm 0.05$, it is not very surprising to find cluster structures char-

Table 1. Cluster fractal dimensions, $d_f|_h$, and average ratios $\langle r_{gxy} \rangle / \langle r_{gz} \rangle |_h$ as a function of the Peclet number. h refers to the *top*, the *middle* and the *bottom* regions. The last column indicates whether the system percolates at the prism base.

Pe	$d_f _{top}$	$d_f _{middle}$	$d_f _{bottom}$	$\langle r_{gxy} \rangle / \langle r_{gz} \rangle _h$	$\langle r_{gxy} \rangle / \langle r_{gz} \rangle _h$	$\langle r_{gxy} \rangle / \langle r_{gz} \rangle _h$	percolation
1	—	—	1.67 ± 0.05	1.01 ± 0.01	0.99 ± 0.03	0.90 ± 0.02	Yes
0.1	1.88 ± 0.07	1.89 ± 0.06	1.74 ± 0.05	1.00 ± 0.05	1.01 ± 0.02	0.95 ± 0.02	Yes
0.01	1.80 ± 0.06	1.83 ± 0.06	1.82 ± 0.05	0.99 ± 0.05	1.00 ± 0.02	0.99 ± 0.02	Yes
0.001	1.82 ± 0.06	1.84 ± 0.06	1.81 ± 0.05	1.02 ± 0.05	1.00 ± 0.02	1.01 ± 0.02	No
0.0001	1.83 ± 0.06	1.80 ± 0.06	1.82 ± 0.05	1.00 ± 0.05	0.99 ± 0.02	1.00 ± 0.02	No
0	1.78 ± 0.06	1.74 ± 0.06	1.76 ± 0.05	0.99 ± 0.05	1.00 ± 0.02	1.00 ± 0.02	No

acterized by fractal dimensions ranging between 1.75 and 1.45 [23,24]. This indicates that for increasing values of the Peclet number, the average cluster size of the settling aggregates that arrive to the prism bottom decreases and hence, most aggregation take place in the bottom region.

The average ratio $\langle r_{gxy} \rangle / \langle r_{gz} \rangle |_h = \langle r_{gx} \rangle / \langle r_{gz} \rangle |_h + \langle r_{gy} \rangle / \langle r_{gz} \rangle |_h / 2$ obtained for different Peclet numbers is shown in table 1. As explained in section 2, this quantity accounts for the average shape of the clusters. In case that $\langle r_{gx} \rangle / \langle r_{gz} \rangle > 1$, the clusters tend to be elongated in the z direction and when $\langle r_{gx} \rangle / \langle r_{gz} \rangle < 1$ the clusters are shorter. For the upper regions, it is observed no significative deviation from unity even for the higher Peclet numbers. This indicates that the clusters do not show a preferential growth direction. This is in good agreement with Allain et. al. experimental observations [1,19]. Nevertheless, our results do not agree with Gonzalez findings [2]. For Peclet numbers as high as 0.1 and for much more concentrated systems ($\phi = 0.01$), Gonzalez found that clusters grow faster in the sedimentation direction. This is very likely to occur since clusters move mostly downwards. For diluted systems, on the other hand, when the Peclet number is as high as 0.1, the clusters settle so fast that they have not the opportunity to grow before arriving to the prism base. This fact explains why we do not obtain $\langle r_{gx} \rangle / \langle r_{gz} \rangle$ significatively larger than unity for the upper regions. The same argument is also valid to explain the differences between the fractal dimensions obtained by Gonzalez and by us. For the lower region and where the sediment grows, for the highest Peclet numbers we obtain $\langle r_{gx} \rangle / \langle r_{gz} \rangle$ lower than unity. This is a consequence of the fact that the aggregation is taking place mostly in the prism bottom, in which the z direction motion is restricted. Hence, the sediment grow covering the base of the prism producing a local two dimensional percolation. This kind of percolation, as shown in table 1, occurs only for the largest values of the Peclet number.

4 Conclusions

The coupled aggregation and sedimentation process were simulated by considering a large prism with no periodical boundary conditions for the sedimentation direction. Three equally sized and mutually excluded regions were defined for studying their time evolution of the cluster size distribution. We found that for the upper regions the shape of the time evolution of oligomers narrows due to

the effect of Stokes velocity. On the contrary, their population dependence on time shows a double peak for the bottom region as a consequence of those settling clusters that arrives at the prism base. The time evolution of the weigh average cluster size also change its behavior depending on the region. While it shows a peak for the upper regions, it becomes a monotonously increasing function for the bottom region. Furthermore, the limiting value of 4 was obtained for its slope for increasing values of the Peclet number.

The cluster structure was also studied by means of measuring the cluster radii of gyration. In agreement with the experiments performed by Allain et. al., we obtained that there is not a preferential growth direction. In addition, we also found an increase in the fractal dimension for increasing the Peclet number and for the upper regions. For the bottom region, however, a decrease in the fractal dimension and the preferential growing directions parallel to the prism base were found for increasing the Peclet number. This is explained as a consequence of the restricted motion of those settling clusters that have already arrived the prism base. Finally, one may conclude that increasing the Peclet number makes the system to increase its tendency to produce a two dimensional percolation at the prism base.

References

1. C. Allain, M. Cloitre, M. Wafra, Phys. Rev. Lett. **74**, (1995) 1478.
2. A. E. Gonzalez, Phys. Rev. Lett. **86**, (2001) 1243.
3. J. Lyklema, *Fundamentals of Interface and Colloid Science. Volume I: Fundamentals*, (Academic Press, London, 1991).
4. R. J. Hunter, *Foundations of Colloid Science*, (Clarendon Press, Oxford, 1987).
5. M. von Smoluchowski, Phys. Z. **17**, (1916) 557.
6. M. von Smoluchowski, Z. Phys. Chem. **92**, (1917) 129.
7. M. Y. Lin, R. Klein, H. M. Lindsay, D. A. Weitz, R. C. Ball, P. Meakin, Phys. Rev. Lett. **A41**, (1990) 2005.
8. M. Y. Lin, H. M. Lindsay, D. A. Weitz, R. Klein, R. C. Ball, P. Meakin, Phys. Condens. Matter **2**, (1990) 3093.
9. D. A. Weitz, M. Oliveria, Phys. Rev. Lett. **52**, (1984) 1433.
10. P. Meakin, Phys. Rev. Lett. **51**, (1983) 1119.
11. P. Meakin, F. Family, Phys. Rev. A **36**, (1987) 5498.
12. F. Family, P. Meakin, T. Vicsek, J. Chem. Phys. **83**, (1985) 4144.
13. A. E. González, Phys. Rev. Lett. **71**, (1993) 2248.

14. M. Lach-hab, A. E. González, E. Blaisten-Barojas, *Phys. Rev. E.* **54**, (1996) 5456.
15. W. B. Russel, D. A. Saville, W. R. Schowalter, *Colloidal Dispersions* (Cambridge University Press, Cambridge, 1989).
16. G. K. Batchelor, *J. Fluid Mech.* **119**, (1982) 379.
17. G. K. Batchelor, C. S. Wen, *J. Fluid Mech.* **124**, (1982) 495.
18. S. B. Grant, J. Ha Kim, C. Poor, *J. Colloid Interface Sci.* **238**, (2001) 238.
19. C. Allain, M. Cloitre, F. Parisse, *J. Colloid Interface Sci.* **178**, (1996) 411.
20. A. E. González, F. Leyvraz, in *Proceedings of the Statistical Mechanics in Physics and Biology Symposium of the MRS 1996 Fall Meeting*, edited by D. Wirtz and T. C. Halsey (Materials Reserch Society, Pittsburgh, 1997).
21. M. L. Broide, R. J. Cohen, *Phys. Rev. Lett.* **64**, (1990) 2026.
22. G. Odriozola, M. Tirado-Miranda, A. Schmitt, F. Martínez-López, J. Callejas-Fernández, R. Martínez-Garía, R. Hidalgo-Álvarez, *J. Colloid Interface Sci.* **240**, (2001) 90.
23. A. Marmur, *J. Colloid Interface Sci.* **72**, (1979) 41.
24. A. Moncho-Jordá, G. Odriozola, F. Martínez-López, A. Schmitt, R. Hidalgo-Álvarez, *Eur. Phys. J. E* **5**, (2001) 471.
25. A. Schmitt, G. Odriozola, A. Moncho-Jordá, J. Callejas-Fernández, R. Martínez-García, R. Hidalgo-Álvarez, *Phys. Rev. E* **62**, (2000) 8335.